Materials and Design 169 (2019) 107687

Contents lists available at ScienceDirect

Materials and Design

journal homepage: www.elsevier.com/locate/matdes

Programmable super elastic kirigami metallic glasses

S.H. Chen [a,b], K.C. Chan [a,*], D.X. Han [a], L. Zhao [a], F.F. Wu [c]

[a] Advanced Manufacturing Technology Research Centre, Department of Industrial and Systems Engineering, The Hong Kong Polytechnic University, Hung Hom, Kowloon, Hong Kong
[b] School of Mechanical Engineering, Hefei University of Technology, Hefei 230009, China
[c] School of Materials Science and Engineering, Liaoning University of Technology, Jinzhou 121001, China

HIGHLIGHTS

- Programmable stretchability reaching 317% and a super elasticity larger than 277% are achieved in kirigami metallic glasses (MGs).
- The design of circle-shaped node-cuts significantly affects the elastic performance of kirigami MGs.
- The super elasticity of kirigami MGs is attributed to the elastic bending of kirigami elements.

GRAPHICAL ABSTRACT

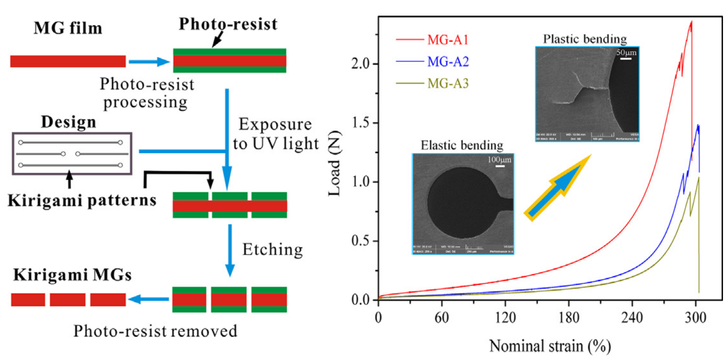

ARTICLE INFO

Article history:
Received 12 January 2019
Received in revised form 2 March 2019
Accepted 3 March 2019
Available online 4 March 2019

Keywords:
Kirigami
Metallic glass
Elasticity
Stretchability
Metamaterials

ABSTRACT

The elastic performance of kirigami metallic glasses (MGs) plays a key role for their applications as potential mechanical metamaterials, however, the mechanisms on how to achieve programmable large elasticity in these kirigami MGs are still unknown. In this work, kirigami MGs, with programmable stretchability reaching 317%, were fabricated, demonstrating super elasticity larger than 277%. The high stretchability and super-elasticity are mainly attributed to the elastic out-of-plane bending of the kirigami elements rather than rigid deformation. The super elastic kirigami MGs can be developed for use as high stretchable mechanical/functional metamaterials/devices, such as wearable sensors and stretchable electronics.

1. Introduction

Building on the assemblies of micro/nano architecture, mechanical metamaterials have programmable structures and unprecedented, intriguing characteristics such as bistability, and nonlinear, negative and extreme properties [1–13]. For example, architectured low porosity auxetic metamaterials can demonstrate negative Poisson's ratio [5], hollow-tube ceramic nanolattice structures have ultra-light and ultra-strong properties [4], and hybrid hierarchical metamaterials exhibit tensile elasticity larger than 20% [10]. By use of the ancient art of paper cutting, kirigami structures with programmable strains are being used to engineer the properties of certain mechanical metamaterials, especially aiming for high stretchability. It has been reported that kirigami nanocomposites (GO-PVA) have increased strains from 4% to 370%, demonstrating great application potential in stretchable electronic and optoelectronic devices [14]. In order to obtain outstanding mechanical/functional properties, kirigami structures have been created in a

* Corresponding author.
E-mail address: kc.chan@polyu.edu.hk (K.C. Chan).

https://doi.org/10.1016/j.matdes.2019.107687

wide range of materials, such as Kapton/GaAs laminates [15], integrated lithium-ion batteries [16], Cr/Parylene C nanocomposites [17], Poly (dimethylsiloxane) [18], plastic sheets [19], paper-based triboelectric nanogenerators [20], Si/polymer nanomembranes [21] and graphene [22]. The kirigami structures have potential applications for stretchable/flexible devices, such as batteries, supercapacitors, electrodes, and conductors [23–28]. However, in the practical applications of stretchable devices, it is important to maintain elasticity for keeping the mechanical and functional performance. Kirigami structures making use of traditional materials possess non-negligible strain energy loss, resulting in decreased cycle life [29]. For example, after 1000 loading cycles, the GO-PVA nanocomposite kirigami structure had strain energy loss of about 18% [14] and the Kapton-based kirigami solar tracker also demonstrated decreased strain energy up to about 74% [15]. Such limitation has significantly impeded the wide applications of kirigami materials with requisite properties.

As a unique class of alloys with stochastic atomic order, metallic glasses (MGs) have relatively-large elastic limit of about 2% and high strength approaching the theoretical values [30,31]. MGs have great potential for applications as structural materials, especially for elastic applications [32–35]. With the designed bending behavior, some elastic MG structures have demonstrated excellent elastic energy storability [36–39]. Recently, the authors fabricated four kinds of MG kirigami structures, two with simple straight and two with simple curved patterns, and studied the strain-energy-loss behavior of the structures [40]. It was reported that the maximum elasticity was 198%, with an ultra-small strain energy loss <3% after 1000 loading cycles [40]. Although elasticity is a key factor influencing the strain-energy-loss behavior of kirigami MGs, how to achieve programmable large elasticity in kirigami MGs has not yet been reported. Moreover, there is a need to better understand the underlying deformation mechanisms for the high stretchability and large elasticity of kirigami MGs. In this work, we have introduced new kirigami patterns to the MG films to achieve programmable super-elasticity. The underlying deformation mechanisms for the high stretchability were analyzed, and strategies for achieving super elasticity in kirigami MGs are proposed. The present work explores the development of meta-materials using metallic materials. By inheriting the superior mechanical properties of metals, the metal-based mechanical metamaterials could obtain outstanding mechanical/functional properties, for example, the super elasticity and the ultra-small strain energy loss in kirigami MGs. These kirigami MGs could directly be used to develop stretchable devices, or be engineered to a variety of substrates for flexible functional devices, such as optoelectronics, electronics and sensors, opening up a broader range of applications for stretchable mechanical metamaterials.

2. Materials and methods

MG films, of about 20 μm thickness with nominal composition of $Fe_{73.5}Si_{13.5}B_9Cu_1Nb_3$ (at.%), were synthesized by rapid quenching of the melted alloys onto a high-speed roller. The amorphous atomic structures were confirmed using standard X-ray diffraction (XRD) analysis. Kirigami MGs were fabricated using photochemical machining (PCM), as shown in the diagram in Fig. 1a [40]. Two layers of photo-resist were firstly spread on the surface of the MG films. After exposure to UV light, kirigami patterns were fabricated in the photo-resist layers. The kirigami structures were then patterned onto MG films through etching, and the kirigami MGs were finally obtained by removing the photo-resist layers. In the present work, various new circle-shaped node-cuts (A1-A3, B1-B3, C1-C3 and D1-D3) were introduced to the four kinds of simple kirigami patterns (A-D), as shown in Fig. 1b. Mechanical tests of the kirigami MGs were conducted on an Instron 3344 materials testing machine at a loading rate of 20 mm/min., using a load cell of $\pm$10 N. 100 sets of data per second were collected for each loading curve. The surface of the deformed kirigami MGs was examined using scanning electron microscopy (SEM) on a TESCAN VEGA3 scanning electron microscope.

3. Results

3.1. High stretchability

Although MGs are known to have certain unique mechanical properties, most MG communities have limited plastic strains, especially under tensile loading. By introducing kirigami patterns, the present kirigami MGs demonstrate large nominal strains, ranging from 173% to 317%. The load-nominal strain curve of a typical A1 kirigami MG is given in Fig. 2, where three stages of deformation can be observed. In stage I, the kirigami structure deforms in a rigid regime within the plane of the film, as shown at point H in the magnified curve. Here, the nominal strain is relatively-small and negligible when compared with the fracture strain of 296%. When loading proceeds, the deformation mode of the kirigami structure transits from rigid in-plane deformation to out-of-plane bending and rotation (point J at stage II). Due to the small film-thickness/cut-distance ratio, an obvious load drop during the transition of deformation modes from stage I to stage II, as shown in the paper-based kirigami structures, was not observed for the present kirigami MGs [40,41]. At this stage, a wide plateau with a relatively small increasing rate of loading was observed till reaching a strain of about 230%. In stage III, the kirigami structures were further stretched, resulting in the rapid increase of the load (point K). It can be seen that the high stretchability of the kirigami MGs was mainly achieved by the out-of-plane deformations in stages II and III.

The influencing factors on the stretchability of kirigami MGs were examined by varying the element shape, size and node shape of the kirigami patterns, where the curved elements (patterns A, B, and C), varying cut-distances (patterns A and D) and circle-shaped node-cuts (patterns A2 to A3) were tailored (Fig. 1b). As shown in Fig. 3a, the fracture strains of the A1, B1 and C1 kirigami MGs are 296%, 297% and 297%, respectively. However, with the increase of the cut-distance, from d_1 to d_4, in the A1 and D1 kirigami MGs, the fracture strain decreased significantly from 296% to 175%. The A2-D2 and A3-D3 specimens showed similar trends to the A1-D1 kirigami MGs. Additionally, as seen in Fig. 3b and Fig. SI1 in the Supplementary Materials, with varying circle-shaped node-cuts, the kirigami MGs did not show an obvious enhancement in the stretchability. It can thus be concluded that the stretchability of the kirigami MGs is not significantly dependent on the change of the element shapes and the circle-shaped node-cuts, except the cut-distance. Nevertheless, although the achievement of high stretchability is beneficial for obtaining higher elastic limit, the elastic performance of kirigami MGs is also affected by the bearing loads. Referring to Fig. 3, the bearing load of the kirigami MGs is influenced by all the element shapes, cut-distances and the sizes of the circle-shaped node cuts. The decrease of bearing loads can result in smaller stress-concentration orders at the nodes, which can lead to better elastic performance.

3.2. Super elasticity

Differing from solid materials where the elastic strains can be measured from the linear stage of the stress-strain curves or by ultrasonic methods, the transition of deformation modes from in-plane deformation to out-of-plane bending/rotation makes it challenging to characterize the nominal elastic limit from the load-strain curves. The elasticity of kirigami MGs was characterized using step-by-step observations [40]. An example of the B3 kirigami MG at a nominal strain of 277% is shown in Fig. SI2 in the Supplementary Materials. By comparing the loading and unloading curves, it can be seen that the unloading curve almost matches the loading curves identically, which suggests that the B3 kirigami MG has an elastic strain limit larger than 277%. Using similar methods, the elastic strain limits of all groups of kirigami MGs are listed

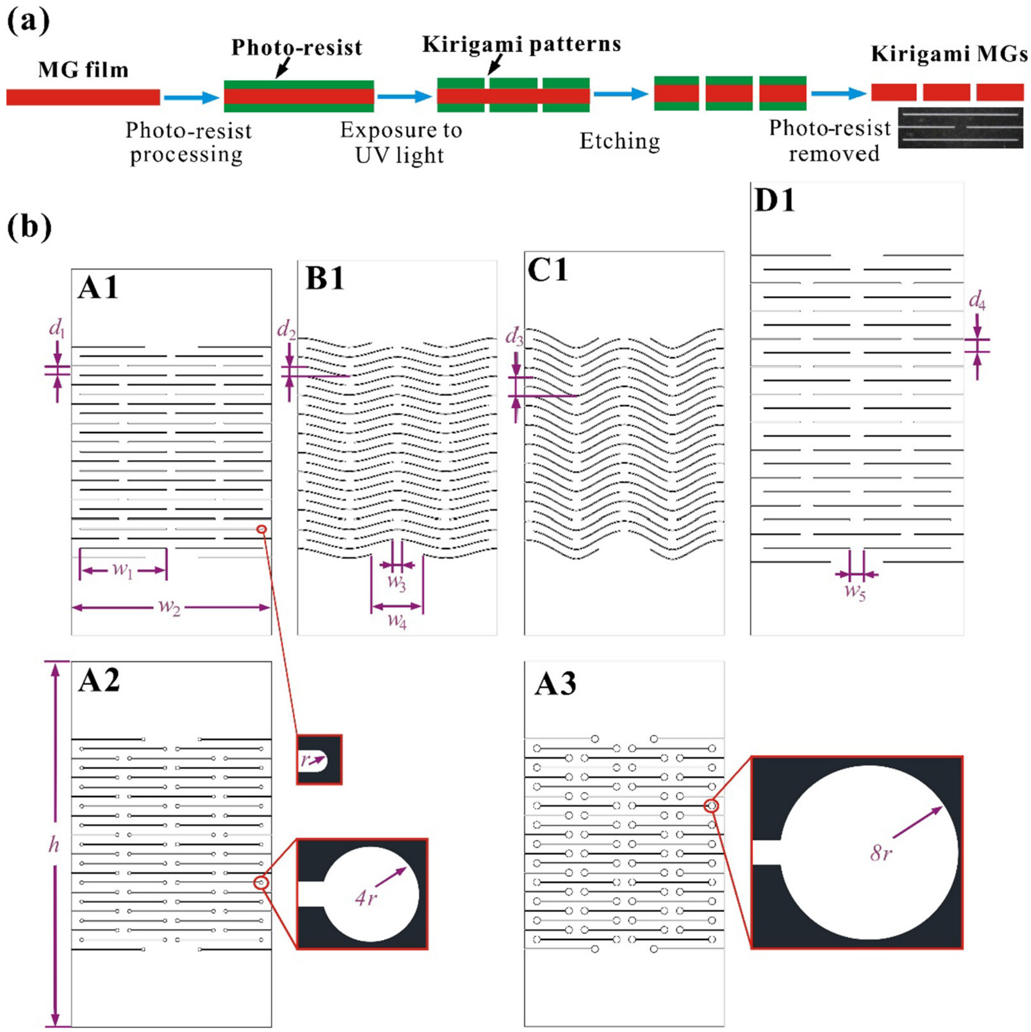

Fig. 1. The PCM of kirigami MGs, where (a) shows the fabrication process, and (b) gives four kinds kirigami patterns (A_1-D_1) as well as varying circle-shaped node-cuts (A1-A3). $d_1 = d_2 =$ 1 mm; $d_3 = 2$ mm; $d_4 = 1.5$ mm; $w_1 = 10$ mm; $w_2 = 23$ mm; $w_3 = 1$ mm; $w_4 = 6$ mm; $w_5 = 1.5$ mm, $h = 42.1$ mm and $r = 0.05$ mm.

in Table 1. As compared with the ~2% elasticity of the bulk form of MGs, the kirigami MGs demonstrate super elastic performance with the largest elasticity larger than 277%. Further to the previous work of the authors reported in Ref. [40], the effect of cut-distance and curved elements on the change of the elastic performance is discussed in detail in the present study. Based on the effects of the influencing factors on the stretchability of kirigami MGs, we firstly examined the specimens with different cut-distances (groups A and D), where significant differences on the stretchability were observed, regardless of the sizes of the circle-shaped node-cuts (A1-A3 and D1-D3). For example, in Fig. 3a, the group A1 kirigami MG has a wide plateau in stage II deformation, which is even larger than the fracture strain of the group D1 specimen. Therefore, it is reasonable to find that group A kirigami MGs have much larger elastic limits than group D specimens. Since the effect of cut-distances on the stretchability of kirigami structures has been studied by Isobe and Okumura [41], the present paper will focus on the effect of curved element and circle-shaped node-cuts on the stretchability of kirigami MGs. For the effect of curved elements (groups A-C), an obvious increase of elasticity in these specimens was observed, including the specimens with circle-shaped node-cuts. Regarding the fact that the specimens with curved elements have similar stretchability as compared with the specimens with straight elements, the relatively-larger elastic limits of the kirigami MGs with curved elements may be due to the decrease of the bearing load (Fig. 3a). With similar stretchability, a relatively-lower bearing load may result in less stress concentrations for the plastic deformation, leading to the improvement of the elastic performance. Such a phenomenon can also be observed in the specimens with circle-shaped node-cuts, where the specimens with larger cut radii also demonstrate better elastic performance, for example, C3 > C2 > C1, despite the achievement of similar stretchability (Fig. 3 and Fig. SI1 in the Supplementary Materials).

In the compression tests of the bulk samples of MGs, large strain energy loss occurred through plastic deformation (Fig. SI3a in the Supplementary Materials). However, for kirigami MGs with super elasticity, an ultra-small strain energy loss was observed when the loading proceeded to the plastic deformation stage. For example, the load-nominal strain curve of an A1 kirigami MG at a large nominal strain of 288% is given in Fig. SI3b in the Supplementary Materials. The unloading curve returns to a nominal strain of about 7%, and only a small amount of strain energy (24.72%) is accommodated by plastic deformation. The elastic strain energy loss data (E_L) of all the groups of specimens at the varying nominal strains (ε_{el}) are also listed, as shown in Table 1. With increase of the radii of the circle-shaped node-cuts, the specimens have decreased strain energy loss. As compared with the A1 kirigami MGs, the A2 specimen has a smaller strain energy loss of about 12.21%. This value is further decreased in the A3 specimen, with only a 1.26% strain energy loss. The other groups of specimens show similar trends with the change of the circle-shaped node-cuts, where with larger circle radii at the nodes, the kirigami structures have significantly improved the elastic strain energy storability. This is because the

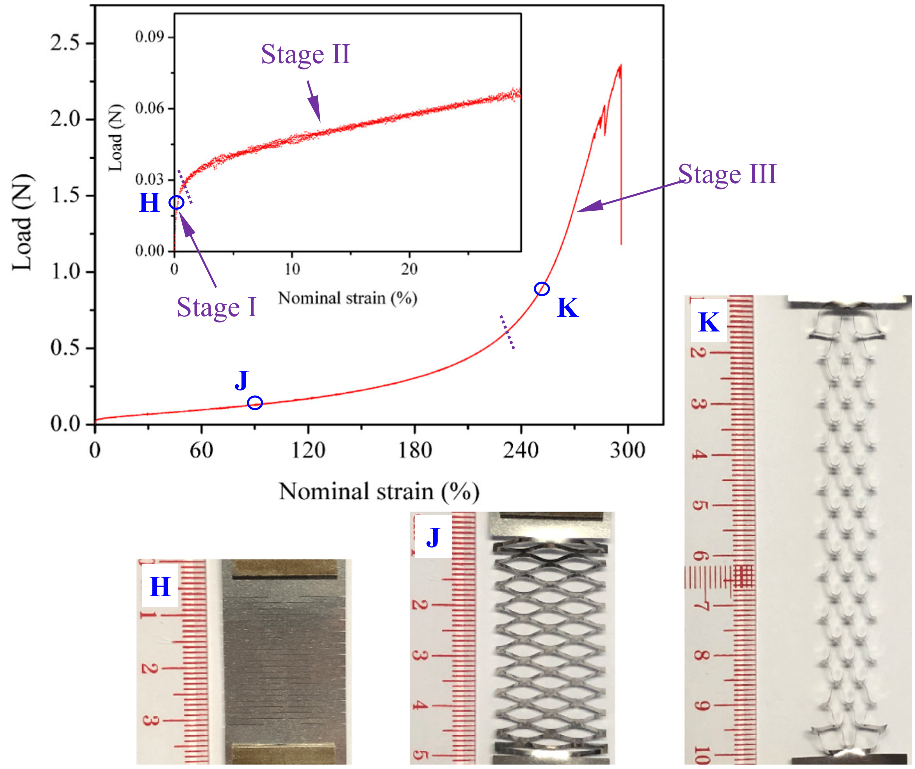

Fig. 2. The load-nominal strain curve of an A1 specimen, where three different deformation stages were observed. The inset shows the change of deformation modes at a higher magnification. The optical images show the typical deformation behavior of the specimens at the points H, J, and K, respectively, at different stages.

kirigami MGs with larger circle-shaped cut radii have larger elasticity (Table 1), and at the same time, lower bearing loads of these kirigami MGs can lead to smaller orders of plastic deformation at the nodes. Since the strain energy loss data were collected at varying nominal strains (ε_{el}), for different kirigami patterns, the effect of the kirigami patterns on the change of the strain energy loss values is not compared quantitatively here. However, according to the elasticity of the group A-C specimens, as well as the typical strain energy loss data, such as A2, B2 and C2, the kirigami patterns with curved elements tend to have smaller strain energy loss.

4. Discussion

The excellent elastic performance of kirigami MGs is associated with the second stage (stage II) of deformation, where out-of-plane bending and rotation of the struts play a dominant role. For the kirigami structures with a cut-distance (d_0) far less than the cut-width (w_0), the deflection of the element (δ_d) is also considered as being far less than the cut-width (w_0), and the bending energy of the kirigami element can be described as the following expression [41]:

$$U\,(\Delta) = \varphi U(\delta_d) \tag{1}$$

where Δ is the axial displacement, φ is a constant relating to the number of the cuts, and $U(\delta_d)$ is the deformation energy of an element with a deflection distance δ_d. The deflection of the element, δ_d, can be approximately determined by the relationship [41]:

$$\delta_d{}^2 = (\Delta/N + d_0)^2 - d_0{}^2 \tag{2}$$

where N is the number of cuts along the h direction as shown in Fig. 1, with cut-distance of d_0 (d_1 or d_4 for the present kirigami MGs). For groups A and D kirigami MGs with the same N, at a certain axial displacement (Δ), the group D specimens have larger cut-distance ($d_4 > d_1$), and therefore require larger deformation energy. More deformation energy being dissipated by the group D kirigami MGs brings to larger stress concentration orders at the nodes, which agrees well with the larger bearing loads, as shown in Fig. 3a. A higher stress concentration order at the nodes will definitely cause the rapid yielding of the nodes, leading to smaller nominal elastic limit. While for groups B and C kirigami MGs with curved elements, under same axial displacement (Δ), it necessitates less energy to achieve the same bending displacement (δ_d), and thus causes the accommodation of less mechanical energy, resulting in larger elasticity. For the kirigami MGs with circle-shaped node-cuts, the increase of the circle radii at the nodes causes the decrease of the "cut-distance" (d_0), and then results in less mechanical energy being accumulated during the loading process. Thus, it can be concluded that programmable large elasticity of the kirigami MGs can be achieved by tailoring the appropriate bending energy of the element through the design of the kirigami patterns, for example, the pattern sizes (cut-distance), geometries (element shapes) and node-cut optimizations in the present work.

The deformation modes of the kirigami structures can be categorized into the rigid deformation (Mode-1), elastic bending of the element (Mode-2), and plastic bending of the element (Mode-3), as shown in the schematic diagram in Fig. 4. The rigid deformation (Mode-1) occurs in stage I of the kirigami MGs, while for bulk samples, they also deform following such a mode. The mechanical energy is dissipated by the plastic deformation of the material after yielding, and large amount of strain energy loss then occurs after the unloading process. For rigid MGs, brittle failure usually occurs for the majority of MG communities (an SEM image of a fractured example is shown in Fig. 4). However, for the kirigami MGs, buckling of the elements occurs at a bearing load far less than the yield point of the parent MGs (rigid samples). Due to the out-of-plane bending of the kirigami element, large orders of stress concentration occur at the nodes. The apparent "yielding" of the kirigami structures is due to the plastic deformation at the nodes. Before the apparent "yielding" point, the kirigami MGs deform as elastic bending, which comprise the main elastic plateau of the kirigami MGs (Mode-2). After "yielding", plastic deformation occurs at the stress-concentrated

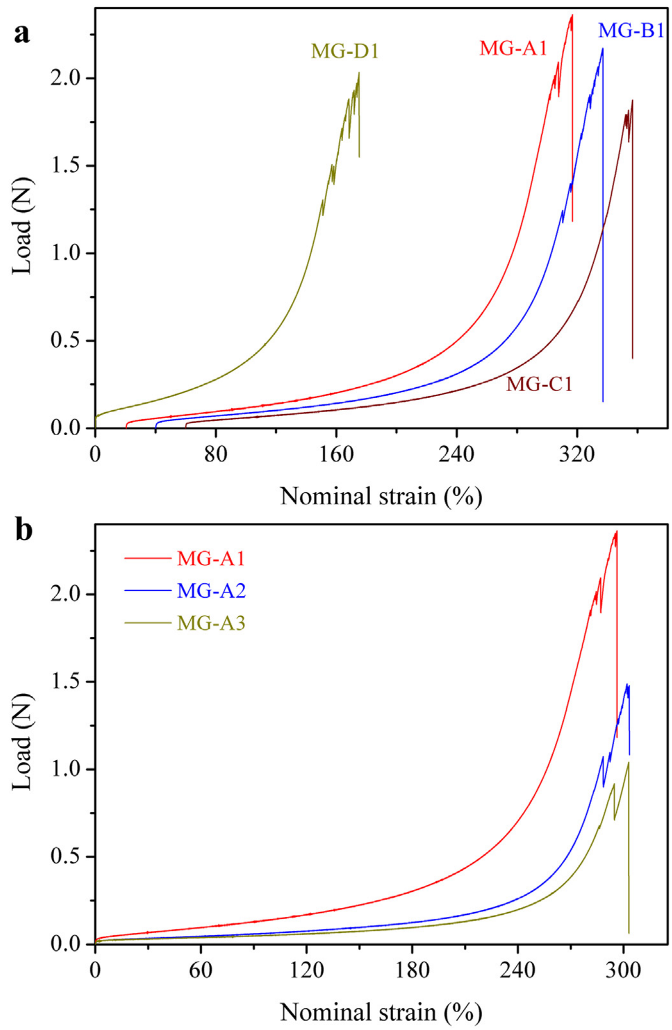

Fig. 3. (a) The comparison of the load-nominal strain curve of groups A1-D1 kirigami MGs. (b) Deformation behavior of group A kirigami MGs with varying circle-shaped node-cuts.

regions at the nodes, while most parts of the kirigami MGs are still in an elastic state (the formation of shear bands is also given in Fig. 4), resulting in the ultra-small strain energy loss after the unloading process, as shown in Fig. SI3 in the Supplementary Materials.

Although the present kirigami MGs have super elasticity, and some of them even have elasticity larger than 277%, the elastic performance of kirigami MGs can be further improved by designing kirigami patterns with smaller bending energy of the elements. Besides the tailoring of

Table 1
The nominal elastic strains (ε_e) and the strain energy losses (E_L) of the kirigami MGs, where ε_{el} is the nominal strain at which the strain energy loss data (E_L) were collected. The nominal elastic strain data of A1-D1 specimens were collected from Ref. [40].

Pattern	ε_e (%)	E_L (%)	ε_{el} (%)
A1	>165[40]	24.72	288
A2	>205	12.21	288
A3	>247	1.26	288
B1	>198[40]	16.02	277
B2	>237	2.11	277
B3	>277	–	277
C1	>190[40]	5.01	266
C2	>228	0.49	266
C3	>266	–	266
D1	>85[40]	6.07	142
D2	>99	0.39	142
D3	>113	0.34	142

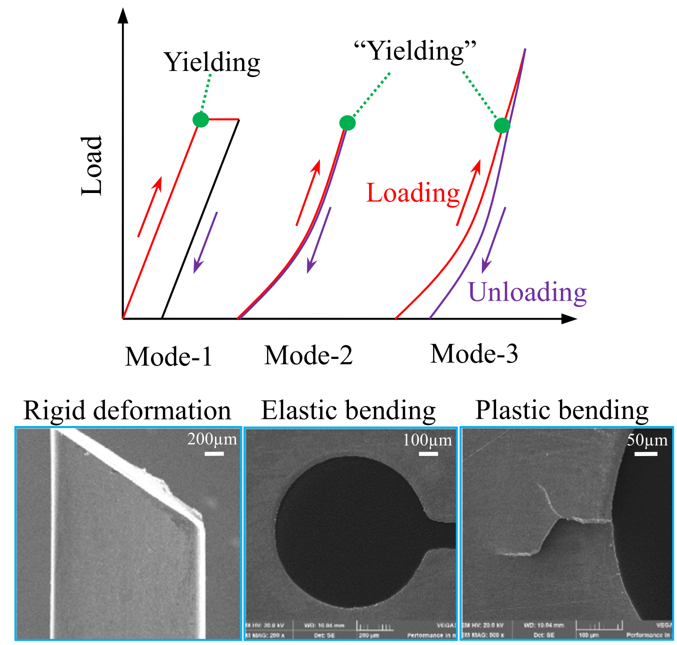

Fig. 4. Schematic diagram showing three kinds of deformation modes: rigid deformation (Mode-1), elastic bending (Mode-2) and plastic bending (Mode-3), where following SEM images are corresponding deformed examples.

smaller cut-distances, curved elements and circle-shaped node-cuts mentioned in the present work, some other methods which can optimize the bending energy of the elements may also be helpful, for example, the design of more complex-shaped kirigami patterns [14], and the tuning of micro cuts [18] and the pattern parameters [19,41]. With super elasticity, kirigami MGs are useful for designing mechanical/functional metamaterials, such as the radar grating components [17] and solar tracking panels [15]. Kirigami MGs can also be used as substrates for developing some functional devices with high stretchability, like the wearable strain sensors [42], super stretchable conductors [43], and stretchable batteries [16,44] and electronics [45–47].

5. Conclusions

By introducing kirigami patterns into MG films, kirigami MGs with high stretchability approaching 327% were fabricated using photochemical machining (PCM). The kirigami MGs exhibited programmable super elastic performance with some values larger than 277%. The effect of cut-distances, curved elements and circle-shaped node-cuts of the kirigami patterns on the stretchability and elasticity of kirigami MGs was investigated. The super elastic performance is mainly attributed to the elastic bending of the kirigami elements. With appropriate design and optimization of the kirigami patterns, the super elasticity behavior of kirigami MGs can be further enhanced. The design of programmable super-elastic kirigami MGs opens up a new window for developing metallic metamaterials with superior mechanical/functional properties, for example, in solar tracking and radar grating systems. The kirigami MGs can also be used as substrates for a wide range of stretchable optoelectronic/electronic devices/sensors to maintain stable functionality within a longer cycle life.

CRediT authorship contribution statement

S.H. Chen: Conceptualization, Methodology, Data curation, Formal analysis, Visualization, Writing - original draft, Writing - review & editing. **K.C. Chan:** Conceptualization, Writing - review & editing. **D.X. Han:** Data curation, Writing - review & editing. **L. Zhao:** Data curation, Writing - review & editing. **F.F. Wu:** Writing - review & editing.

Acknowledgements

The work described in this paper was fully supported by a grant from the Research Grants Council of the Hong Kong Special Administrative Region, China (Project No. PolyU 15222017).

Additional information

Competing financial interests

The authors declare no competing financial interests.

Appendix A. Supplementary data

Supplementary data to this article can be found online at https://doi.org/10.1016/j.matdes.2019.107687.

References

[1] Z.G. Nicolaou, A.E. Motter, Mechanical metamaterials with negative compressibility transitions, Nat. Mater. 11 (2012) 608–613, https://doi.org/10.1038/NMAT3331.
[2] B. Florijn, C. Coulais, M. van Hecke, Programmable mechanical metamaterials, Phys. Rev. Lett. 113 (2014), 175503. https://doi.org/10.1103/PhysRevLett.113.175503.
[3] X.Y. Zheng, H. Lee, T.H. Weisgraber, M. Shusteff, J. DeOtte, E.B. Duoss, J.D. Kuntz, M.M. Biener, Q. Ge, J.A. Jackson, S.O. Kucheyev, N.X. Fang, C.M. Spadaccini, Ultralight, ultrastiff mechanical metamaterials, Science 344 (2014) 1373–1377, https://doi.org/10.1126/science.1252291.
[4] L.R. Meza, S. Das, J.R. Greer, Strong, lightweight, and recoverable three-dimensional ceramic nanolattices, Science 345 (2014) 1322–1326, https://doi.org/10.1126/science.1255908.
[5] M. Taylor, L. Francesconi, M. Gerendas, A. Shanian, C. Carson, K. Bertoldi, Low porosity metallic periodic structures with negative Poisson's ratio, Adv. Mater. 26 (2014) 2365–2370, https://doi.org/10.1002/adma.201304464.
[6] J.L. Silverberg, J.H. Na, A.A. Evans, B. Liu, T.C. Hull, C.D. Santangelo, R.J. Lang, R.C. Hayward, I. Cohen, Origami structures with a critical transition to bistability arising from hidden degrees of freedom, Nat. Mater. 14 (2015) 389–393, https://doi.org/10.1038/NMAT4232.
[7] K. O'Brien, H. Suchowski, J. Rho, A. Salandrino, B. Kante, X.B. Yin, X. Zhang, Predicting nonlinear properties of metamaterials from the linear response, Nat. Mater. 14 (2015) 379–383, https://doi.org/10.1038/NMAT4214.
[8] J. Paulose, B.G.G. Chen, V. Vitelli, Topological modes bound to dislocations in mechanical metamaterials, Nat. Phys. 11 (2015) 153–156, https://doi.org/10.1038/NPHYS3185.
[9] A.A. Zadpoor, Mechanical meta-materials, Mater. Horiz. 3 (2016) 371–381, https://doi.org/10.1039/c6mh00065g.
[10] X.Y. Zheng, W. Smith, J. Jackson, B. Moran, H.C. Cui, D. Chen, J.C. Ye, N. Fang, N. Rodriguez, T. Weisgraber, C.M. Spadaccini, Multiscale metallic metamaterials, Nat. Mater. 15 (2016) 1100–1106, https://doi.org/10.1038/NMAT4694.
[11] H.B. Fang, S.C.A. Chu, Y.T. Xia, K.W. Wang, Programmable self-locking origami mechanical metamaterials, Adv. Mater. 30 (2018), 1706311. https://doi.org/10.1002/adma.201706311.
[12] M. Kaur, T.G. Yun, S.M. Han, E.L. Thomas, W.S. Kim, 3D printed stretching-dominated micro-trusses, Mater. Des. 134 (2017) 272–280, https://doi.org/10.1016/j.matdes.2017.08.061.
[13] C. Moes, G. Hibbard, Development of melt-stretching technique for manufacturing fully-recyclable thermoplastic honeycombs with tunable cell geometries, Mater. Des. 141 (2018) 67–80, https://doi.org/10.1016/j.matdes.2017.12.025.
[14] T.C. Shyu, P.F. Damasceno, P.M. Dodd, A. Lamoureux, L.Z. Xu, M. Shlian, M. Shtein, S.C. Glotzer, N.A. Kotov, A kirigami approach to engineering elasticity in nanocomposites through patterned defects, Nat. Mater. 14 (2015) 785–789, https://doi.org/10.1038/NMAT4327.
[15] A. Lamoureux, K. Lee, M. Shlian, S.R. Forrest, M. Shtein, Dynamic kirigami structures for integrated solar tracking, Nat. Commun. 6 (2015), 8092. https://doi.org/10.1038/ncomms9092.
[16] Z.M. Song, X. Wang, C. Lv, Y.H. An, M.B. Liang, T. Ma, D. He, Y.J. Zheng, S.Q. Huang, H.Y. Yu, H.Q. Jiang, Kirigami-based stretchable lithium-ion batteries, Sci. Rep. 5 (2015), 10988. https://doi.org/10.1038/srep10988.
[17] L.Z. Xu, X.Z. Wang, Y. Kim, T.C. Shyu, J. Lyu, N.A. Kotov, Kirigami nanocomposites as wide-angle diffraction gratings, ACS Nano 10 (2016) 6156–6162, https://doi.org/10.1021/acsnano.6b02096.
[18] Y.C. Tang, G.J. Lin, S. Yang, Y.K. Yi, R.D. Kamien, J. Yin, Programmable kiri-kirigami metamaterials, Adv. Mater. 29 (2017), 1604262. https://doi.org/10.1002/adma.201604262.
[19] A. Rafsanjani, K. Bertoldi, Buckling-induced kirigami, Phys. Rev. Lett. 118 (2017), 084301. https://doi.org/10.1103/PhysRevLett.118.084301.
[20] C.S. Wu, X. Wang, L. Lin, H.Y. Guo, Z.L. Wang, Paper-based triboelectric nanogenerators made of stretchable interlocking kirigami patterns, ACS Nano 10 (2016) 4652–4659, https://doi.org/10.1021/acsnano.6b00949.
[21] Y.H. Zhang, Z. Yan, K.W. Nan, D.Q. Xiao, Y.H. Liu, H.W. Luan, H.R. Fu, X.Z. Wang, Q.L. Yang, J.C. Wang, W. Ren, H.Z. Si, F. Liu, L.H. Yang, H.J. Li, J.T. Wang, X.L. Guo, H.Y. Luo, L. Wang, Y.G. Huang, J.A. Rogers, A mechanically driven form of kirigami as a route to 3D mesostructures in micro/nanomembranes, Proc. Natl. Acad. Sci. U. S. A. 112 (2015) 11757–11764, https://doi.org/10.1073/pnas.1515602112.
[22] M.K. Blees, A.W. Barnard, P.A. Rose, S.P. Roberts, K.L. McGill, P.Y. Huang, A.R. Ruyack, J.W. Kevek, B. Kobrin, D.A. Muller, P.L. McEuen, Graphene kirigami, Nature 524 (2015) 204–207, https://doi.org/10.1038/nature14588.
[23] D.P. Qi, Z.Y. Liu, M. Yu, Y. Liu, Y.X. Tang, J.H. Lv, Y.C. Li, J. Wei, L. Bo, Z. Yu, X.D. Chen, Highly stretchable gold nanobelts with sinusoidal structures for recording electrocorticograms, Adv. Mater. 27 (2015) 3145–3151, https://doi.org/10.1002/adma.201405807.
[24] Y.H. Zhang, Y.G. Huang, J.A. Rogers, Mechanics of stretchable batteries and supercapacitors, Curr. Opin. Solid State Mater. Sci. 19 (2015) 190–199, https://doi.org/10.1016/j.cossms.2015.01.002.
[25] Q. Ma, Y.H. Zhang, Mechanics of fractal-inspired horseshoe microstructures for applications in stretchable electronics, J. Appl. Mech. 83 (2016), 111008. https://doi.org/10.1115/1.4034458.
[26] Z.Y. Liu, X.T. Wang, D.P. Qi, C. Xu, J.C. Yu, Y.Q. Liu, Y. Jiang, B. Liedberg, X.D. Chen, High-adhesion stretchable electrodes based on nanopile interlocking, Adv. Mater. 29 (2017), 1603382. https://doi.org/10.1002/adma.201603382.
[27] Y.Q. Liu, K. He, G. Chen, W.R. Leow, X.D. Chen, Nature-inspired structural materials for flexible electronic devices, Chem. Rev. 117 (2017) 12893–12941, https://doi.org/10.1021/acs.chemrev.7b00291.
[28] J.X. Wang, G.F. Cai, S.H. Li, D.C. Gao, J.Q. Xiong, P.S. Lee, Printable superelastic conductors with extreme stretchability and robust cycling endurance enabled by liquid-metal particles, Adv. Mater. 30 (2018), 1706157. https://doi.org/10.1002/adma.201706157.
[29] S.H. Chen, H.Y. Cheng, K.C. Chan, G. Wang, Metallic glass structures for mechanical-energy-dissipation purpose: a review, Metals 8 (2018) 689, https://doi.org/10.3390/met8090689.
[30] M.M. Trexler, N.N. Thadhani, Mechanical properties of bulk metallic glasses, Prog. Mater. Sci. 55 (2010) 759–839, https://doi.org/10.1016/j.pmatsci.2010.04.002.
[31] J. Plummer, W.L. Johnson, Is metallic glass poised to come of age? Nat. Mater. 14 (2015) 553–555, https://doi.org/10.1038/nmat4297.
[32] W.L. Johnson, Bulk glass-forming metallic alloys: science and technology, MRS Bull. 24 (1999) 42–56, https://doi.org/10.1557/S0883769400053252.
[33] A. Inoue, N. Nishiyama, New bulk metallic glasses for applications as magnetic-sensing, chemical, and structural materials, MRS Bull. 32 (2007) 651–658, https://doi.org/10.1557/mrs2007.128.
[34] B. Sarac, J. Ketkaew, D.O. Popnoe, J. Schroers, Honeycomb structures of bulk metallic glasses, Adv. Funct. Mater. 22 (2012) 3161–3169, https://doi.org/10.1002/adfm.201200539.
[35] B. Sarac, J. Schroers, Designing tensile ductility in metallic glasses, Nat. Commun. 4 (2013), 2158. https://doi.org/10.1038/ncomms3158.
[36] R.D. Conner, W.L. Johnson, N.E. Paton, W.D. Nix, Shear bands and cracking of metallic glass plates in bending, J. Appl. Phys. 94 (2003) 904–911, https://doi.org/10.1063/1.1582555.
[37] G. Kumar, D. Rector, R.D. Conner, J. Schroers, Embrittlement of Zr-based bulk metallic glasses, Acta Mater. 57 (2009) 3572–3583, https://doi.org/10.1016/j.actamat.2009.04.016.
[38] Z. Liu, W. Chen, J. Carstensen, J. Ketkaew, R.M.O. Mota, J.K. Guest, J. Schroers, 3D metallic glass cellular structures, Acta Mater. 105 (2016) 35–43, https://doi.org/10.1016/j.actamat.2015.11.057.
[39] C. Minnert, M. Kuhnt, S. Bruns, A. Marshal, K.G. Pradeep, M. Marsilius, E. Bruder, K. Durst, Study on the embrittlement of flash annealed $Fe_{85.2}B_{9.5}P_4Cu_{0.8}Si_{0.5}$ metallic glass ribbons, Mater. Des. 156 (2018) 252–261, https://doi.org/10.1016/j.matdes.2018.06.055.
[40] S.H. Chen, K.C. Chan, T.M. Yue, F.F. Wu, Highly stretchable kirigami metallic glass structures with ultra-small strain energy loss, Scr. Mater. 142 (2018) 83–87, https://doi.org/10.1016/j.scriptamat.2017.08.037.
[41] M. Isobe, K. Okumura, Initial rigid response and softening transition of highly stretchable kirigami sheet materials, Sci. Rep. 6 (2016), 24758. https://doi.org/10.1038/srep24758.
[42] H.J. Xian, C.R. Cao, J.A. Shi, X.S. Zhu, Y.C. Hu, Y.F. Huang, S. Meng, L. Gu, Y.H. Liu, H.Y. Bai, W.H. Wang, Flexible strain sensors with high performance based on metallic glass thin film, Appl. Phys. Lett. 111 (2017), 121906. https://doi.org/10.1063/1.4993560.
[43] Y. Wang, C.X. Zhu, R. Pfattner, H.P. Yan, L.H. Jin, S.C. Chen, F. Molina-Lopez, F. Lissel, J. Liu, N.I. Rabiah, Z. Chen, J.W. Chung, C. Linder, M.F. Toney, B. Murmann, Z. Bao, A highly stretchable, transparent, and conductive polymer, Sci. Adv. 3 (2017), e1602076. https://doi.org/10.1126/sciadv.1602076.
[44] S. Xu, Y.H. Zhang, J. Cho, J. Lee, X. Huang, L. Jia, J.A. Fan, Y.W. Su, J. Su, H.G. Zhang, H.Y. Cheng, B.W. Lu, C.J. Yu, C. Chuang, T.I. Kim, T. Song, K. Shigeta, S. Kang, C. Dagdeviren, I. Petrov, P.V. Braun, Y.G. Huang, U. Paik, J.A. Rogers, Stretchable batteries with self-similar serpentine interconnects and integrated wireless recharging systems, Nat. Commun. 4 (2013) 1543, https://doi.org/10.1038/ncomms2553.
[45] J. Byun, E. Oh, B. Lee, S. Kim, S. Lee, Y. Hong, A single droplet-printed double-side universal soft electronic platform for highly integrated stretchable hybrid electronics, Adv. Funct. Mater. 27 (2017), 1701912. https://doi.org/10.1002/adfm.201701912.
[46] Y.J. Ma, M. Pharr, L. Wang, J. Kim, Y.H. Liu, Y.G. Xue, R. Ning, X.F. Wang, H.U. Chung, X. Feng, J.A. Rogers, Y. Huang, Soft elastomers with ionic liquid-filled cavities as strain isolating substrates for wearable electronics, Small 13 (2017), 1602954. https://doi.org/10.1002/smll.201602954.
[47] A. Miyamoto, S. Lee, N.F. Cooray, S. Lee, M. Mori, N. Matsuhisa, H. Jin, L. Yoda, T. Yokota, A. Itoh, M. Sekino, H. Kawasaki, T. Ebihara, M. Amagai, T. Someya, Inflammation-free, gas-permeable, lightweight, stretchable on-skin electronics with nanomeshes, Nat. Nanotechnol. 12 (2017) 907–913, https://doi.org/10.1038/NNANO.2017.125.